Chemical Bonding as a New Avenue for Controlling Excited-State Properties and Excitation Energy Transfer Processess in Zinc Phthalocyanine-Fullerene Dyads

Zi-Wen Li¹, Jia-Jia Yang¹, Xiang-Yang Liu², Wei-Hai Fang¹, Haobin Wang^{3*}, and Ganglong Cui^{1*}

- [1] College of Chemistry, Beijing Normal University, Beijing 100875, China
 - E-mail: ganglong.cui@bnu.edu.cn
- [2] College of Chemistry and Material Science, Sichuan Normal University, Chengdu 610068, China
- [3] Department of Chemistry, University of Colorado Denver, Denver, Colorado 80217-3364, United States

E-mail: haobin.wanq@ucdenver.edu

Supporting information for this article is given via a link at the end of the document.

Abstract: Whether chemical bonding can regulate excited-state and optoelectronic properties of molecular donor-acceptor dyads has been largely elusive. In this work we employ time-dependent density functional theory (TDDFT) and TDDFT-based nonadiabatic dynamics method to explore excited-state properties of covalently bonded zinc phthalocyanine (ZnPc)-fullerene (C₆₀) dyads with 6-6 [or 5-6] bonding configuration in which ZnPc is bonded to two carbon atoms shared by the two hexagonal rings [or a pentagonal and a hexagonal ring] in C₆₀. In both cases, the locally excited (LE) states on ZnPc are spectroscopically bright. However, their different chemical bondings differentiate the electronic interactions between ZnPc and C₆₀. In the 5-6 bonding configuration the LE states on ZnPc are much higher in energy than the LE states on C₆₀. Thus, the excitation energy transfer from ZnPc to C₆₀ is thermodynamically favorable. On the other hand, in the 6-6 bonding configuration such a process is inhibited because the LE states on ZnPc are the lowest ones. More detailed mechanisms are elucidated from nonadiabatic dynamics simulations. In the 6-6 bonding configuration, no excitation energy transfer has been observed. In contrast, in the 5-6 bonding configuration, several LE and charge-transfer (CT) excitons have been identified to participate in the energy transfer process. Further analysis reveals that the photoinduced energy transfer is mediated by a CT exciton, such that electron and hole transfer processes take place in a concerted but asynchronous manner during the excitation energy transfer. It is found that high-level electronic structure methods including exciton effects are indispensable to accurately describe photoinduced energy and electron transfer processes. Furthermore, the present work opens up new avenues for regulating excited-state properties by means of chemical bonding. This has significant implications for the rational design of excellent heterojunction interfaces for a variety of optoelectronic devices with superior performances.

Introduction

Photoinduced electron and energy transfer processes are ubiquitous in natural photosynthesis, for example plant and bacterial photosynthetic systems, in which primary photochemical events involve capturing and funneling sunlight by a group of well-organized chromophores called "anatenna complexes" and promoting electron transfer using the funneled light into the

reaction center via a cascade of electron and energy transfer processes. 1-3 The high efficiency of natural photosynthetic systems to convert sunlight into chemical energy has inspired basic research in artificial photosynthesis. Over the past few decades, a large number of light-harvesting donor-acceptor dyads, following the "design" by nature, have been synthesized as artificial photosynthetic antenna and reaction-center model compounds to mimic the early photoevents of natural photosynthesis. These donor-acceptor dyads have been found useful in light-electricity conversion, light-fuel production, and construction of optoelectronic devices.4-8 Obviously these applications are closely related to the photoinduced electron and energy transfer processes between the donor and the acceptor moieties in the dyads. As a consequence, understanding such photoinduced processes is of great importance to both fundamental research and practical applications. This has led to numerous experimental and computational studies on exploring excited-state properties and photoinduced electron and energy transfer dynamics in various molecular donor-acceptor dyads.9-16

Molecular complexes of zinc phthalocyanine (ZnPc) and C60 (C60) are among the most studied donor-acceptor dyads, in particular those formed through noncovalent van der Waals interactions. 17-26 In these ZnPc-C60 complexes, ZnPc always serves as a donor while C60 serves as an acceptor. Upon photoirradiation, an exciton is first populated within ZnPc. It is followed by exciton dissociation and charge separation at the interface, which eventually produces a charge-separated state. Interestingly, previous experiments found that the interfacial excited-state properties and photoinduced exciton and chargeseparation dynamics are heavily influenced by the interfacial orientation of ZnPc and C60. For example, the face-on orientation increases the photocurrent signal by about 50% and improves power conversion substantially from 1.5% to 2.8% in comparison with the edge-on orientation, which is inferred from the improved interfacial charge transfer dynamics.²⁷

In addition, there is another type of ZnPc-C60 molecular dyads in which both ZnPc and C60 are linked through strong covalent bonds. 28-32 These complexes are better viewed as intramolecular donor-acceptor systems. Several experimental groups have made significant contributions to synthesizing them and studying their physiochemical and excited-state properties, for example Guldi and D'Souza groups to name just a few. 33-41 Experiments have found that the chemical nature of covalent

linkers in such ZnPc-C60 molecular systems can change the electronic interaction between ZnPc and C60 and affect their excited-state properties. Nevertheless, the relevant microscopic mechanisms are still far from being fully understood.

On the computational side, some excellent works have been reported in recent years for exploring interfacial electronic structures and charge transfer dynamics of the ZnPc-C60 molecular complexes. However, most of them focused on the noncovalently-bonded molecular complexes formed via van der Waals interactions. 42-46 Theoretical studies on covalently-bonded ZnPc-C60 molecular systems have been rare. Recently, Santos and Wang carried out Ehrenfest dynamics simulations to explore photoinduced electron and hole transfer dynamics between ZnPc and C60 in two different covalently bonded ZnPc-C60 systems. 47 Their results reveal that the organic linkers connecting ZnPc and C60 have remarkable influence on the photoinduced charge injection processes.47 However, the mean-field dynamics approach ignores exciton effects that can affect the efficiency of charge separation into free electrons and holes at interfaces. Moreover, molecular-orbital (MO)-based mean-field methods are not suitable for simulating excitation energy transfer due to the lack of electron-hole interactions. Thus, it is unclear whether excitation energy transfer is involved in the above ZnPc-C60 dyads. Finally, the MO-based mean-field approximation may not correctly capture the role of charge-transfer excitons in excitedstate electron and energy transfer, so that whether charge transfer excitons are involved is entirely elusive in such kind of mean-field simulations.

Most importantly, previous studies only explored one covalent bonding configuration between C60 and ZnPc. According to our study, however, there are two different configurations (see Fig. 1). In the first configuration, the two oxygen atoms of ZnPc are bonded to the two carbon atoms shared by two hexagonal rings of C60 (termed "6-6" bonding configuration in this paper). In the second configuration, the two oxygen atoms are bonded to the two carbon atoms shared by a pentagonal and a hexagonal ring of C60 (termed "5-6" bonding configuration in this paper). Until now, it is unclear whether: (1) these two different bonding configurations have similar effects on the excited-state property and photoinduced energy and electron transfer dynamics; (2) chemical bonding can open up a new avenue for controlling the excited-state properties of molecular donor-acceptor dyads. The insights gained from studying these two questions will undoubtedly enhance our understanding on how to improve excited-state energy and electron transfer efficiencies, which will help the rational design of molecular donoracceptor dyads and heterojunction interfaces to achieve superior properties of various optoelectronic devices such as solar cells.

Motivated by the above questions, we have carried out the first TDDFT-based nonadiabatic dynamics study to explore the excited-state properties and excitation energy transfer dynamics of the two covalently bonded ZnPc-C60 molecular systems, in which ZnPc is bonded to C60 via either the 5-6 and or the 6-6 bonding configuration as shown in Fig. 1. It should be stressed that the exciton effects are naturally and accurately described by employing the linear-response TDDFT method. A8,49 Based on our simulation results, it is found that these two bonding configurations can induce qualitatively different excited-state properties and lead to two distinct excited-state relaxation dynamics. Specifically, the ZnPc-C60 complex with the 5-6 bonding configuration has very efficient ultrafast excited-state

energy transfer mediated by the charge transfer excitons, whereas the complex with the 6-6 bonding configuration does not exhibit excitation energy transfer at all within the 500 fs simulation time. These new findings clearly demonstrate that chemical bonding can regulate excited-state properties and relaxation dynamics of ZnPc-C60 and may help design novel dyads and

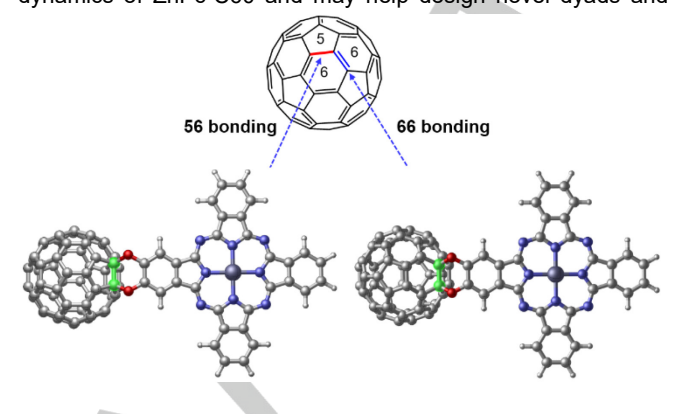


Figure 1. Schematic heterojunction structures of ZnPc and C_{60} with different (left) 5-6 and (right) 6-6 bonding configurations. In the 5-6 bonding configuration, the two oxygen atoms of ZnPc are bonded to two carbon atoms shared by both pentagonal and hexagonal rings; while, in the 6-6 bonding, they are bonded to two carbon atoms shared by two hexagonal rings. Different elements are shown in color.

optoelectronic devices with superior interfacial properties.

Simulation Details

Geometries of the ZnPc-C60 heterojunctions with 5-6 and 6-6 bonding configurations were optimized using the B3LYP+D3 method. $^{50-53}$ For the heavy Zn atoms the inner core electrons were treated with pseudopotentials and the outer valence electrons were described with the LANL2DZ basis sets. The C, H, O, and N atoms were described with the cc-pVDZ basis sets. 54,55 Excitation energies were computed by the TD-CAM-B3LYP method that had been shown to be accurate for the charge transfer excited states. 5 In order to explore the interaction between ZnPc and C60 we have conducted energy decomposition analysis using the combined extended transition state and natural orbitals for chemical valence approach. 57,58 In its framework, the total interaction energy E_{tot} is decomposed into four terms

 $E_{tot}=E_{Pauli}+E_{electro}+E_{orb}+E_{dis}$ where E_{Pauli} refers to the exchange repulsion energy between different fragments due to Pauli's principle; $E_{electro}$ denotes the quasiclassical electrostatic interaction energy between the fragmental charge densities; E_{orb} describes the energy gain due to the orbital mixing of fragments; and E_{dis} corresponds to the dispersion correction energy. Energy decomposition calculations were performed at the B3LYP+D3/TZP level of theory. E_{orb}

In our nonadiabatic dynamics simulations, potential energies, time derivative nonadiabatic couplings, etc. were calculated at the TD-CAM-B3LYP level of theory. The time derivative nonadiabatic couplings between two involved electronic states were numerically computed using our recently implemented algorithm. 60,61 Empirical quantum decoherence correction of Granucci et al. was added in the dynamics simulations. 62 Moreover, nonadiabatic dynamics simulations were performed under the classical path approximation, which was demonstrated to be reasonably accurate for excited-state relaxations without

involving large conformational change and chemical bond forming or breaking. 63-65 Two ZnPc-C60 systems were first heated to three hundred Kelvin and equilibrated for one picosecond using molecular dynamics simulations. A time step of one femtosecond was used for nuclear propagation and a Nosé-Hoover chain thermostat technique (chain length: 5) was used to control the temperature to around three hundred Kelvin in a Born-Oppenheimer-based ground-state canonical molecular dynamics simulation. 6-6,67 Then, a micro-canonical dynamics simulation of two picoseconds was performed from which five hundred initial conditions were randomly generated. Finally, starting from each initial condition, eight hundred trajectories were propagated for five hundred femtoseconds. In order to satisfy the detailed balance condition under the classical path approximation, electronic hop rejection and velocity rescaling were replaced by scaling transition probabilities $p_{\mathbf{k}\mathbf{j}}(t)$ with a Boltzmann factor of $b_{kj} = exp\left(-\frac{E_j - E_k}{k_B T}\right)\!,$ which had been demonstrated to work well in many nonadiabatic dynamics simulations of materials. 68-70

All DFT and TDDFT calculations with the CAM-B3LYP functional were carried out using GAUSSIAN09.⁷¹ Energy decomposition calculations were performed with ADF2016.^{72,73} Ground-state molecular dynamics simulations were conducted with the PBE method⁷⁴ as well the DZVP-MOLOPT-SR-GTH basis sets and Goedecker-Teter-Hutter pseudopotentials.⁷⁵⁻⁷⁸ These molecular dynamics simulations were carried out using the QUICKSTEP module implemented in CP2K.^{79,80} All nonadiabatic dynamics simulations were conducted using our own GTSH package.⁸¹ Electronic transition density analyses on TDDFT results were calculated using MULTIWFN3.6.⁸²

Results and Discussion

The molecular complexes of C60 and ZnPc covalently bonded via 5-6 and 6-6 configurations were optimized at the B3LYP+D3 level of theory, as shown in Fig. 1. It is clear that the two oxygen atoms of ZnPc are covalently bonded to C60 in both complexes. Overall, these two structures look similar except for the bonding position of the two carbon atoms in C60. In order to describe their interactions in a more quantitative way, we have performed energy decomposition analysis based on natural orbitals from the chemical valence method with respect to both the ZnPc and C60 fragments. It is obvious from Table 1 that the interaction is much stronger in the 6-6 configuration than that in the 5-6 configuration, specifically, 196.8 kcal/mol vs. 159.3 kcal/mol at the B3LYP+D3 level of theory. Thus, the 6-6 configuration is more stable in gas phase. Nevertheless, the 5-6 configuration is still possible under certain conditions, e.g. in crystals. Further analysis on the four types of interactions related to the energy decomposition analysis reveals that the difference between the 5-6 and 6-6 configurations mainly arises from the orbital mixing interaction (-488.9 vs. -512.9 kcal/mol) and the dispersion interaction (-83.6 vs. -102.48 kcal/mol). The other two types of interactions, i.e. Pauli and electrostatic interactions are comparable for the two configurations (see Table 1). Since the 6-6 configuration has much stronger orbital and dispersion interactions than its 5-6 counterpart, it is understandable why the 6-6 configuration is more stable.

To further explore the excited-state properties of the two complexes, we carried out TD-DFT calculations using a widely used range-separated exchange-correlation functional, i.e. CAM-B3LYP, which had been shown to work well for charge-transfer excited states.⁸³ The simulated absorption spectra of the two

configurations are shown in Fig. S1, in which nearly same profiles with a peak at around 630 nm were observed. Moreover, in both cases electronic absorptions are exclusively originated from the locally excited (LE) states within ZnPc because of their large oscillator strengths. Neither the LE states within C60 nor the charge transfer (CT) excited states between ZnPc and C60 contributed significantly (very small oscillator strengths). More interestingly, the relative positions of the corresponding LE and CT excited states are different between the 5-6 and 6-6 configurations, as shown in Fig. 2. For the former configuration, the LE states within ZnPc are much higher in energy (S3 and S4) than the CT state between C60 and ZnPc and the LE state within C60 (S2 and S1). Therefore, the nonadiabatic transitions from the LE states of ZnPc to the LE state of C60, via their CT state, are thermodynamically favorable and may occur efficiently. In these processes one may expect that the LE state of C60 will eventually be populated and the CT state between ZnPc and C60 serves as an intermediate. In contrast, the LE states within ZnPc are the lowest ones for the 6-6 configuration. Thus, once they are populated in the Franck-Condon region, the up-conversion processes to the higher LE state of C60 and the relevant CT states are difficult. As a consequence, the molecular donoracceptor complexes of ZnPc and C60 with different covalent bonding configurations exhibit distinctly different excited-state

Table 1. B3LYP+D3 Calculated Energy-Decomposition Analysis based on Natural Orbitals for Chemical Valence Method (in kcal/mol).

Configuration	total	Pauli	Electro.	Orb.	Dis.
5-6	-159.3	741.5	-328.2	-488.9	-83.6
6-6	-196.8	747.3	-328.7	-512.9	-102.8

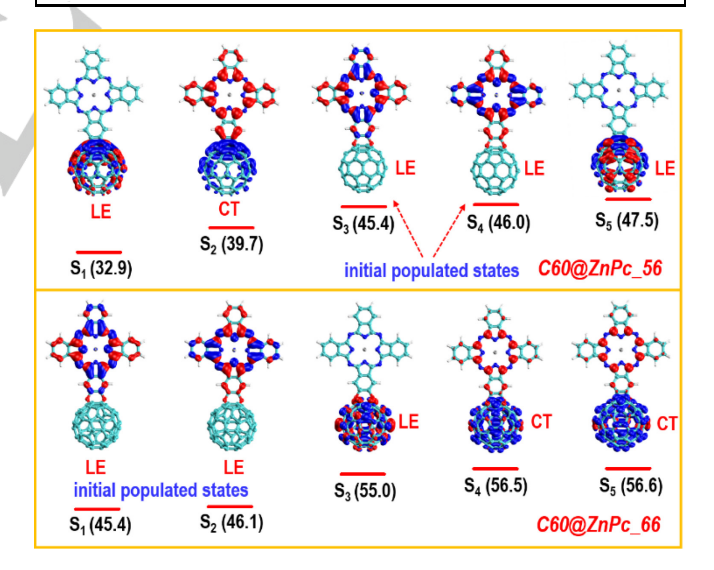


Figure 2. Electronic transition density of the lowest five electronically excited singlet states in the 5-6 bonding (up) and 6-6 bonding (bottom) configurations (charge accumulation in red and charge deletion in blue). Also shown are excitation energies (in kcal/mol)

properties.

The above different excited-state properties between the 5-6 and 6-6 configurations will undoubtedly induce different excited-state dynamics and thus different energy transfer and charge separation. In order to obtain quantitative information about these

dynamical processes, we have performed TD-CAM-B3LYP nonadiabatic dynamics simulations using Tully's surface-hopping method⁸⁴ to study the excited-state relaxation dynamics of the ZnPc-C60 complexes in the 5-6 and 6-6 configurations.

In our simulation the initial states were the bright LE states within ZnPc. The overall time-dependent electronic wavefunction was linearly expanded from the adiabatic wavefunctions of the excited states of interest, $\Psi(t) = \Sigma_n C_n(t) \Psi_n$, where $C_n(t)$ is the time-dependent coefficient for the nth electronic state. ^81.85 In the linear response TDDFT theory, 86 Ψ_n can be approximated as a linear combination of the singly excited Slater determinants ψ_i^a with coefficients w_{ia}

$$\Psi_n = \sum_{i}^{occ} \sum_{a}^{unocc} w_{ia} \psi_i^a$$

in which MO indices i and a run over the occupied and the unoccupied orbitals, respectively. Such a Slater determinant ψ_i^a can be viewed as an exciton with a hole in the ath unoccupied MO and an electron in the ith occupied MO. After some linear transformations, these MO-based excitons ψ_i^a can be converted to more intuitive, fragment-based LE and CT excitons, e.g. $|C_{60}ZnPC^*>,|C_{60}^*ZnPC^->,$ and $|C_{60}^*ZnPC^+>$ for our presently studied ZnPc-C60 complexes (see the supporting

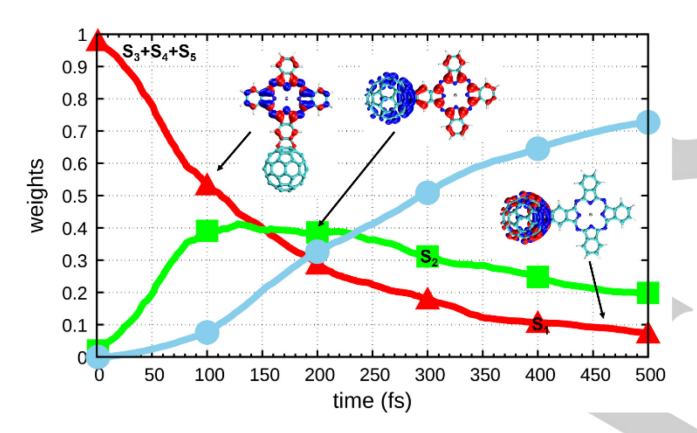


Figure 3. Time-dependent populations of involved electronically excited states S_n (n=1-5). See texts for discussions.

information for details).

Fig. 3 illustrates the time-dependent populations of the participating electronically excited states S_n (n=1-5) from the nonadiabatic dynamics simulation of the ZnPc-C60 complex in the 5-6 bonding configuration. From TDDFT calculations, it is clear that only the LE states within ZnPc have large oscillator strengths and will be populated upon photoirradiation. However, the LE states of ZnPc are very close to that of C60 in energy, for example, 45.4 and 46.0 kcal/mol vs. 47.5 kcal/mol at the Franck-Condon point in Fig. 2. Due to this energy proximity, the initial LE state of ZnPc could be the S₃, S₄, or S₅ state (adiabatic electronic states in ascending energy). In Fig. 3, their populations are combined together (see Fig. S2 for the separated populations). Within 500 fs simulation time, these S₃, S₄, and S₅ populations decrease monotonically to less than 0.1 and the S₁ population increases to more than 0.7 accordingly. By contrast, the S2 population first increases to a maximum of ca. 0.4 at about 100 fs and then slowly decreases to 0.2 at the end of 500 fs simulation.

The above time-dependent populations of the adiabatic electronic states provide useful information for understanding the excited-state relaxation dynamics of the molecular ZnPc-C60

complex. Yet the roles of the LE and CT excitons are still not uncovered. Such knowledge is important for studying photoinduced intramolecular energy and charge transfer dynamics among different fragments (e.g. donors and acceptors) and can be easily extracted in terms of our developed fragmentbased exciton analysis method. Fig. 4 shows the time-dependent weights of $|C_{60}ZnPC^*\rangle$, $|C_{60}^*ZnPC\rangle$, $|C_{60}^+ZnPC^->$, and $|C_{60}^-ZnPC^+|$ > excitons from the nonadiabatic dynamics simulation of the ZnPc-C60 complex in the 5-6 bonding configuration. The initial photoexcitation primarily populates the ZnPc LE exciton $|C_{60}\text{ZnPC}^*\rangle$ (> 90%) with a very small population on the C60 LE exciton $|C_{60}^* ZnPC>$ and nearly no for the $|C_{60}^+ ZnPC^->$ and $|C_{60}^{-}ZnPC^{+}\rangle$ excitons. This agrees with the static electronic structure calculations where the ZnPc LE states have much larger oscillator strengths than the others (panel a in Fig. S1). Once the initial excited states are populated in the Franck-Condon region, the excited-state relaxation proceeds involving three types of excitons, $|C_{60}ZnPC^*>$, $|C_{60}^*ZnPC>$, and $|C_{60}^-ZnPC^+>$. In the first 100 fs, the $|C_{60}\text{ZnPC}^*|$ > population quickly decreases from 0.9 to 0.4 accompanied by some coherent oscillations. Afterwards, it decreases monotonically to < 0.1 until the end of 500 fs simulation. Differently, in the first 20 fs the $|C_{60}^* ZnPC|$ population has a sharp increase to 0.4 but decreases to 0.2 in the following 80 fs. Finally, it gradually grows up to 0.7 at the end of 500 fs simulation. The $|C_{60}^-ZnPC^+>$ population exhibits two different stages. It first sharply increases to 0.4 at 100 fs, and then decreases to 0.2 in the remaining 400 fs simulation time. As expected, the $|C_{60}^+ZnPC^->$ exciton is not involved in the excited-state relaxation dynamics.

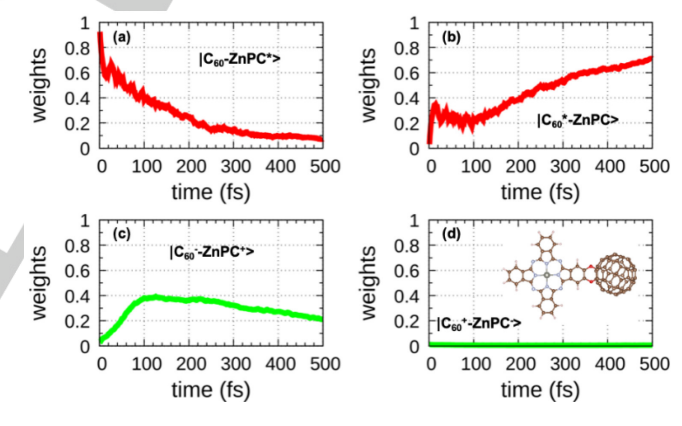


Figure 4. Time-dependent weights of (a-d) different excitons. (a) local exciton within ZnPc; (b) local exciton within C60; (c) charge-transfer exciton from ZnPc to C60; (d) charge-transfer exciton from C60 to ZnPc. See supporting information for simulation details and algorithms for these analyses

We now analyze dynamics in more detail, in particular the turning points observed from the time-dependent populations of $C_{60}^{\ast} \mathrm{ZnPC} >$ and $|C_{60}^{-} \mathrm{ZnPC}^{+} >$. During the first 20 fs, the population of $|C_{60}^{\ast} \mathrm{ZnPC} >$ has a sharp increase to 0.4, consistent with the decrease in the population of $|C_{60}^{\ast} \mathrm{ZnPC}^{\ast} >$ at the same time. This primarily stems from the fact that the LE states of C60 are energetically lower than the LE states of ZnPc in some regions. Nonadiabatic transitions from the LE states of ZnPc to that of C60 take place on an ultrafast timescale (ca. 20 fs) because the three LE states are very close to each other (e.g. 45.4, 46.0, and 47.5 kcal/mol in Fig. 2). Subsequently, both the C60 LE exciton $|C_{60}^{\ast} \mathrm{ZnPC} >$ and the ZnPc LE exciton $|C_{60}^{\ast} \mathrm{ZnPC}^{\ast} >$ will further hop to the lower CT exciton $|C_{60}^{\ast} \mathrm{ZnPC}^{+} >$ (see Fig. 2). Therefore, one can see a clear increase in the $|C_{60}^{\ast} \mathrm{ZnPC}^{+} >$ population reaching

a maximum of 0.4 at 100 fs. However, because the S₁ state is an LE state of C60, $|C_{60}^-\mathrm{ZnPC}^+>$ will eventually be converted to $|C_{60}^*\mathrm{ZnPC}>$. Thus, at the end of the 500 fs simulation time, the $|C_{60}^*\mathrm{ZnPC}>$ population increases to 0.7 whereas the $|C_{60}^-\mathrm{ZnPC}^+>$ population reduces to 0.2.

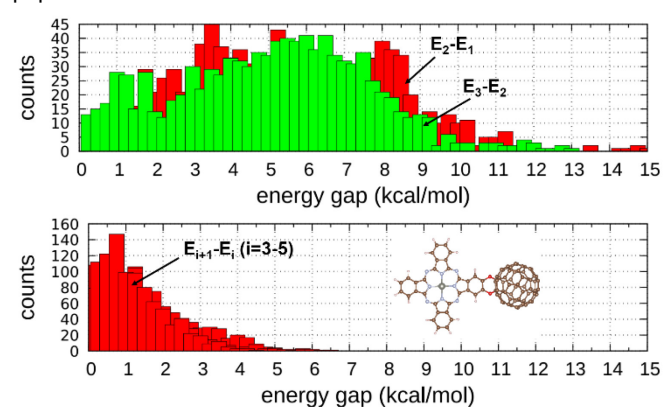


Figure 5. Distributions of energy gaps of E_2 - E_1 , E_3 - E_2 , and E_{i+1} - E_i (i=3-5) in nonadiabatic dynamics simulations

In addition, one can see that the internal conversion processes among the LE states of ZnPc and C60, i.e. S₃, S₄, and S₅, are very efficient and completed within 20 fs. In comparison, those involving the CT state, e.g. from S₃ to S₂ and from S₂ to S₁, are relatively slow. For example, it takes about 400 fs to reduce the $|C_{60}^-ZnPC^+\rangle$ population from 0.4 to 0.2 as shown in panel c of Fig. 4. To rationalize these dynamical differences, in-depth analysis is carried out in terms of the equations of motion of Tully's fewest-switches surface-hopping method, in which energy gaps and nonadiabatic couplings of involved electronic states are in charge of nonadiabatic hoppings. Fig. 5 shows the corresponding distributions of the energy gaps of E₂-E₁, E₃-E₂, and E_{i+1}-E_i (i=3-5). It is clear that the energy gaps are small among the S₃, S₄, and S₅ states. Specifically, the averaged energy gap is smaller than 2.0 kcal/mol and nearly all energy gaps are smaller than 5 kcal/mol.

Moreover, nonadiabatic couplings among these three electronic states i.e. S_3 , S_4 , and S_5 are also very large, as shown in Fig. 6 (see diagonal elements). These large values are reasonable because there is an inverse relation between the energy gaps and nonadiabatic couplings

$$d_{ij} = \frac{\left\langle \Psi_i \middle| \frac{\partial H}{\partial R} \middle| \Psi_j \right\rangle}{E_i - E_i}$$

in which Ψ_i and Ψ_j are the two involved electronic wavefunctions, and E_i and E_j are related energies. Since the $S_3,\ S_4,\$ and S_5 electronic states have very small energy gaps, one can expect the large nonadiabatic couplings in the bottom panel of Fig. 5. Therefore, large nonadiabatic couplings make the internal conversion processes among $S_3,\ S_4,\$ and S_5 ultrafast and complete within 20 fs. By contrast, there are relatively large energy gaps among $S_3,\ S_2,\$ and S_1 in the top panel of Fig. 5. Averaged energy gaps are more than 5.0 kcal/mol. In addition, one can see wide distributions for these energy gaps. These large energy gaps result in relatively small nonadiabatic couplings compared with those related to $S_3,\ S_4,\$ and S_5 (see Fig. 6), which lead to comparably slower excited-state relaxation dynamics among $S_3,\ S_2,\$ and S_1 (see Figs. 3 and 4).

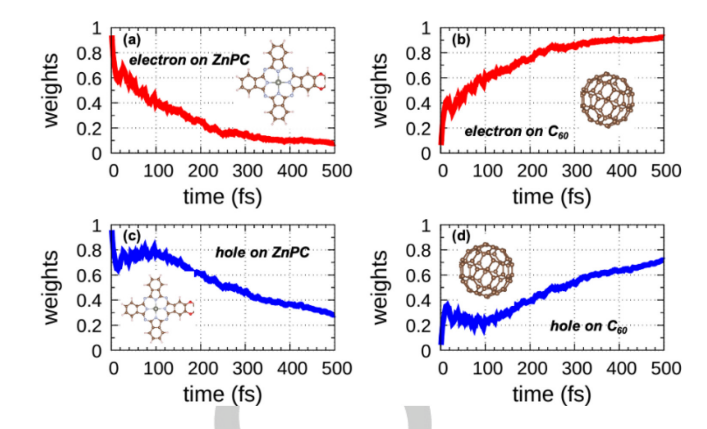


Figure 6. Distribution of averaged nonadiabatic couplings among the five lowest electronic states i.e. S_n (n=1-5) in nonadiabatic dynamics simulations.

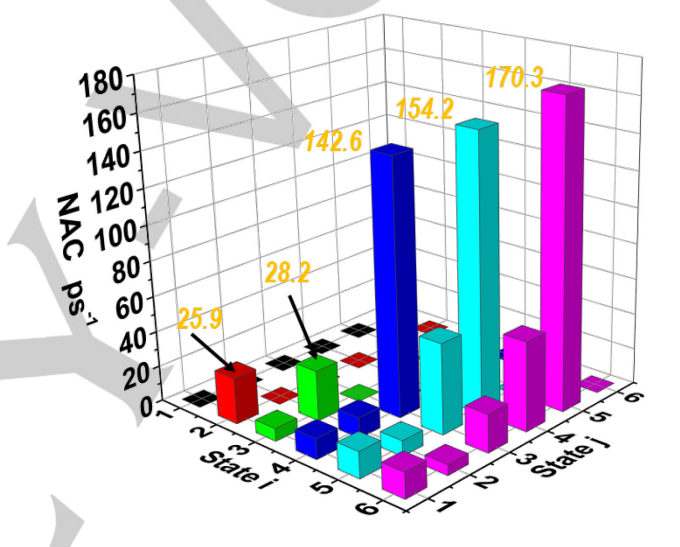


Figure 7. Time-dependent electron and hole amounts on ZnPc and C60 fragments calculated based on nonadiabatic dynamics simulations.

With further linear transformations on the time-dependent fragment-based exciton analysis, one can obtain the underlying dynamical information of the photoinduced electron and hole transfers among the donor and acceptor. This could provide useful information to help design better molecular donor-acceptor systems. Fig. 7 shows the time-dependent electron and hole occupations located on ZnPc and C60. It is found that more than 90% electron and hole occupations are initially located on the same ZnPc fragment, which means that photoirradiation produces LE excitons within ZnPc (see panels a and c). This is consistent with the above time-dependent exciton analysis in Fig. 4. In the first 20 fs, one can see a sharp increase (decrease) in the electron and hole occupations on C60 (ZnPc), which corresponds to the LE exciton transfer from ZnPc to C60 observed at the same time in Fig. 4. Afterwards, electrons continue to travel from ZnPc to C60 with some coherent fluctuations in the first 100 fs, as shown in panels a and b of Fig. 7. Unlike electron transfer, the hole transfer exhibits a complicated behavior after the first 20 fs (see panels c and d). During the next 80 fs, the hole occupation on ZnPc [C60] increases [decreases] from 0.6 to 0.8 [0.4 to 0.2]. This is related to the internal conversion processes from the LE states of ZnPc and C60 to the CT state, which is also observed from the time-dependent populations of the relevant excitons in Fig. 4. Subsequently, holes slowly transfer from ZnPc to C60. Thus, the above nonadiabatic exciton transfer dynamics is a coupled electron and hole transfer process, which takes place in a concerted but asynchronous way. This characteristic is also reflected very well by the calculated exciton sizes in the nonadiabatic dynamics simulations, as shown in Fig. 8. In the beginning, the exciton size is 5.3 Å due to the LE character within ZnPc. After the electron transfer to C60 takes place producing a CT exciton, it gradually increases to 7.6 Å at 100 fs. Finally, the exciton size decreases to 6.0 Å because of the hole transfer to C60 to generate an LE $|C_{60}^*ZnPC>$ exciton.

Unlike the molecular ZnPc-C60 complex in the 5-6 bonding

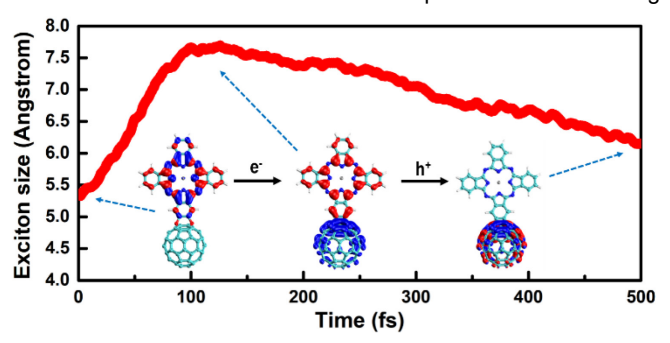


Figure 8. Time-dependent exciton sizes calculated based on nonadiabatic dynamics simulations. Electron and hole are in blue and red. See discussion in text.

configuration, there are no nonadiabatic transitions observed in the nonadiabatic dynamics simulations for the 6-6 bonding configuration (see Fig. S3). Populations of $|C_{60}ZnPC^*>$, $|C_{60}^* ZnPC>, \ |C_{60}^+ ZnPC^->, \ \text{and} \ |C_{60}^- ZnPC^+> \text{do not change at all}$ during the entire 500 fs simulation time (see panels a-d of Fig. S3). Consequently, the distance between the electron and the hole does not vary significantly on ZnPC or C60. The results are in line with the static electronic structure calculations in which the ZnPc LE states are the lowest ones in energy. These two states have significantly larger oscillator strengths and photoirradiation makes them exclusively populated. In this case, nonadiabatic transitions to the higher CT and LE states are unfavorable thermodynamically and therefore do not appear in our dynamics simulations. As a result, neither the excited-state charge separation nor energy transfer is seen in short time (500 fs). The comparison between the 5-6 and 6-6 bonding configurations for the ZnPc-C60 complex highlights the importance of using chemical bonding properties between the ZnPc and C60 moieties to regulate the excited-state properties and relaxation dynamics, and ultimately the photoinduced energy transfer dynamics.

Summary

We have for the first time explored the excited-state properties and photoinduced excited-state energy transfer dynamics of the two covalently-bonded ZnPc-C60 molecular complexes with different bonding configurations between the ZnPc and C60 moieties. In the 6-6 bonding configuration the two oxygen atoms of ZnPc are bonded to the two carbon atoms shared by the two hexagonal rings of C60, whereas in the 5-6 bonding configuration these two oxygen atoms are bonded to the two carbon atoms shared by a pentagonal and a hexagonal ring of C60. TD-CAM-B3LYP calculations show that the LE excited states within ZnPc are spectroscopically bright in both

configurations. However, different chemical bonding properties induce different electronic interactions between ZnPc and C60. As a result, the ZnPc LE states have different energies relative to the CT excited states. In the 5-6 bonding configuration, the LE states on ZnPc are much higher in energy than the LE state on C60 and the CT state between them. Consequently, charge separation and energy transfer are favored thermodynamically. In contrast, for the 6-6 bonding configuration the LE states within ZnPc are the lowest ones, which makes charge separation and energy transfer processes unfavorable because these upconversion processes require considerable energy.

These conclusions are further supported by our TDDFTbased nonadiabatic dynamics simulations. In the 6-6 bonding configuration, no exciton transfer and charge separation are seen within the 500 fs simulation time. In contrast, all these processes are available in the 5-6 bonding configuration. The LE excitons $|C_{60}{\rm ZnPC^*}>$ and $|C_{60}^*{\rm ZnPC}>$, and the CT exciton $|C_{60}^-{\rm ZnPC^+}>$ are involved, with no visible contribution from the CT exciton $|C_{60}^{+}ZnPC^{-}>$. Detailed analysis reveals that the excited-state energy transfer from ZnPc to C60 is mediated by the CT exciton $|C_{60}^-ZnPC^+>$. Because of this CT exciton, electron and hole transfers take place in a concerted but asynchronous manner and both processes are along the same direction from ZnPc to C60. Specifically, the electron transfer process is followed by the hole transfer. This dynamical characteristic is also reflected by the calculated exciton size, which first increases from 5.5 to 7.5 Å due to the electron transfer, and then gradually decreases to 6.0 Å at the end of the 500 fs simulation time because of the subsequent hole transfer. Methodologically, the proved importance of this CT exciton for mediating excited state energy transfer of ZnPc-C60 also underlines the fact that nonadiabatic dynamics simulations with higher-level electronic structure methods and beyond the mean-field approximation are necessary to accurately uncover the role of CT excitons in either excited-state energy or electron transfer dynamics.

Finally, previous experimental studies have found that relative orientations of ZnPc and C60 in noncovalently bonded complexes are very important for regulating the excited-state properties and interfacial electron transfer processes and eventually the power conversion efficiencies of the ZnPc-C60 photovoltaic devices.²⁷ Our present work demonstrates that in addition to the relative orientations, chemical bonding can also be used as a new way to regulate excited-state properties of molecular donor-acceptor dyads, which is crucial for regulating photoinduced energy or electron transfer efficiencies of the donor-acceptor systems. Most importantly, these gained theoretical findings could contribute valuable knowledge to help design excellent interfaces of heterojunctions of a variety of optoelectronic devices such as solar cells to achieve superior properties in future.⁸⁷⁻⁹¹

Acknowledgements

This work has been supported by the NSFC grants 21688102, 21590801, and 21520102005 (G.C. and W.F.) and Sichuan Science and Technology Program grant 2020YJ0161 (X.L.). H.W. acknowledge the support from the national science foundation CHE-1954639.

Supporting Information Available

Simulation details, additional Figures and Tables, and Cartesian coordinates.

Keywords: zinc phthalocyanine • fullerene • excited states • energy transfer • nonadiabatic dynamics

- B. R. Green, W. W. Parson, Eds. Light-Harvesting Antennas in Photosynthesis, Kluwer, Dordrecht, The Netherlands, 2003.
- [2] M. Pessarakli, Ed. Handbook of Photosynthesis, CRC Press LLC, Boca Raton, FL, 2005.
- [3] R. Cogdell, C. Mullineaux, Eds. Photosynthetic Light Harvesting, Springer, Dordrecht, The Netherlands, 2008.
- [4] K. A.Mazzio, C. K.Luscombe, Chem. Soc. Rev. 2015, 44, 78-90.
- [5] J. Zhang, W. Xu, P. Sheng, G. Y. Zhao, D. B. Zhu, Acc. Chem. Res. 2017, 50, 1654-1662.
- [6] G. J. Hedley, A. Ruseckas, I. D. W. Samuel, Chem. Rev. 2017, 117, 796-837.
- [7] M. M. Li, C. B. An, W. Pisula, K. Müllen, Acc. Chem. Res. 2018, 51, 1196-1205.
- [8] G. Y. Zhang, J. B. Zhao, P. C. Y. Chow, K. Jiang, J. Q. Zhang, Z. L. Zhu, J. Zhang, F. Huang, H. Yan, Cells. Chem. Rev. 2018, 118, 3447-3507.
- [9] A. de la Escosura, M. V. Martínez-Díaz, D. M. Guldi, T. Torres, J. Am. Chem. Soc. 2006, 128, 4112-4118.
- [10] C. T. Chapman, W. Liang, X. S. Li, J. Phys. Chem. Lett. 2011, 2, 1189-1192
- [11] A. A. Bakulin, A. Rao, V. G. Pavelyev, P. H. M. van Loosdrecht, M. S. Pshenichnikov, D. Niedzialek, J. Cornil, D. Beljonne, R. H. Friend, Science 2012, 335, 1340-1344.
- [12] S. M. Falke, C. A. Rozzi, D. Brida, M. Maiuri, M. Amato, E. Sommer, A. De Sio, A. Rubio, G. Cerullo, E. Molinari, C. Lienau, *Science* 2014, 344, 1001-1005
- [13] P. B. Deotare, W. Chang, E. Hontz, D. N. Congreve, L. Shi, P. D. Reusswig, B. Modtland, M. E. Bahlke, C. K. Lee, A. P. Willard, V. Bulovic, T. Van Voorhis, M. A. Baldo, *Nat. Mater.* 2015, 14, 1130-1134.
- [14] A. C. Jakowetz, M. L. Bohm, J. B. Zhang, A. Sadhanala, S. Huettner, A. A. Bakulin, A. Rao, R. H. Friend, J. Am. Chem. Soc. 2016, 138, 11672-11679
- [15] D. Fazzi, M. Barbatti, W. Thiel, *J. Am. Chem. Soc.* **2016**, *138*, 4502-4511.
- [16] D. Fazzi, M. Barbatti, W. Thiel, *J. Phys. Chem. Lett.* **2017**, *8*, 4727-4734.
- [17] D. M. Guldi, J. Ramey, M. V. Martínez-Díaz, A. de la Escosura, T. Torres, T. Da Ros, M. Prato, Chem. Commun. 2002, 2774-2775.
- [18] S. Pfuetzner, J. Meiss, A. Petrich, M. Riede, K. Leo, Appl. Phys. Lett. 2009, 94, 253303.
- [19] W. J. Zeng, K. S. Yong, Z. M. Kam, F. R. Zhu, Y. N. Li, Appl. Phys. Lett. 2010, 97, 133304.
- [20] S. Pfuetzner, C. Mickel, J. Jankowski, M. Hein, J. Meiss, C. Schuenemann, C. Elschner, A. A. Levin, B. Rellinghaus, K. Leo, M. Riede, Org. Electron. 2011, 12, 435-441.
- [21] Y. Zhou, T. Taima, T. Miyadera, T. Yamanari, M. Kitamura, K. Nakatsu, Y. Yoshida, Appl. Phys. Lett. 2012, 100, 233302.
- [22] A. Sánchez-Díaz, L. Burtone, M. Riede, E. Palomares, J. Phys. Chem. C 2012, 116, 16384-16390.
- [23] P. A. Lane, P. D. Cunningham, J. S. Melinger, G. P. Kushto, O. Esenturk, E. J. Heilweil, *Phys. Rev. Lett.* 2012, 108, 077402.
- [24] H. J. Kim, J. W. Kim, H. H. Lee, B. Lee, J.-J. Kim Adv. Funct. Mater. 2012, 22, 4244-4248.
- [25] T. Wang, T. R. Kafle, B. Kattel, W.-L. Chan, J. Am. Chem. Soc. 2017, 139, 4098-4106.
- [26] C. Gaul, S. Hutsch, M. Schwarze, K. S. Schellhammer, F. Bussolotti, S. Kera, G. Cuniberti, K. Leo, F. Ortmann, Nat. Mater. 2018, 17, 439-444.
- [27] B. P. Rand, D. Cheyns, K. Vasseur, N. C. Giebink, S. Mothy, Y. P. Yi, V. Coropceanu, D. Beljonne, J. Cornil, J.-L. Brédas, J. Genoe, Adv. Funct. Mater. 2012, 22, 2987-2995.
- [28] D. M. Guldi, A. Gouloumis, P. Vázquez, T. Torres, Chem. Commun. 2002, 2056-2057.

- [29] T. Torres, A. Gouloumis, D. Sanchez-Garcia, J. Jayawickramarajah, W. Seitz, D. M. Guldi, J. L. Sessler, Chem. Commun. 2007, 292-294.
- [30] F. Auras, Y. Li, F. Löbermann, M. Döblinger, J. Schuster, L. M. Peter, D. Trauner, T. Bein, Chem. Eur. J. 2014, 20, 14971-14975.
- [31] S. Zhou, M. Yamamoto, G. A. D. Briggs, H. Imahori, K. Porfyrakis, J. Am. Chem. Soc. 2016, 138, 1313-1319.
- [32] Y. Tamura, D. Kuzuhara, M. Suzuki, H. Hayashi, N. Aratani, H. Yamada, J. Mater. Chem. A 2016, 4, 15333-15342.
- [33] D. M. Guldi, A. Gouloumis, P. Vázquez, T. Torres, V. Georgakilas, M. Prato, J. Am. Chem. Soc. 2005, 127, 5811-5813.
- [34] B. Ballesteros, G. de la Torre, C. Ehli, G. M. A. Rahman, F. Agulló-Rueda, D. M. Guldi, T. Torres, J. Am. Chem. Soc. 2007, 129, 5061-5068.
- [35] G. Bottari, G. de la Torre, D. M. Guldi, T. Torres, Chem. Rev. 2010, 110, 6768-6816.
- [36] C. K. C. Bikram, N. K. Subbaiyan, F. D'Souza, J. Phys. Chem. C 2012, 116, 11964-11972.
- [37] C. B. KC, G. N. Lim, P. A. Karr, F. D'Souza, Chem. Eur. J. 2014, 20, 7725-7735.
- [38] S. K. Das, A. Mahler, A. K. Wilson, F. D'Souza, ChemPhysChem 2014, 15, 2462-2472.
- [39] C. B. KC, G. N. Lim, F. D'Souza, Nanoscale 2015, 7, 6813-6826.
- [40] S. V. Kirner, C. Henkel, D. M. Guldi, J. D. Megiatto, D. I. Schuster, Chemical Science 2015, 6, 7293-7304.
- [41] C. O. Obondi, G. N. Lim, Y. Jang, P. Patel, A. K. Wilson, P. K. Poddutoori, F. D'Souza, J. Phys. Chem. C 2018, 122, 13636-13647.
- [42] S. H. Park, J. G. Jeong, H.-J. Kim, S.-H. Park, M.-H. Cho, S. W. Cho, Y. Yi, M. Y. Heo, H. Sohn, Appl. Phys. Lett. 2010, 96, 013302.
- [43] S. Javaid, M. J. Akhtar, J. Appl. Phys. 2015, 118, 045305.
- [44] S. Javaid, M. J. Akhtar, Appl. Phys. Lett. 2016, 109, 051605.
- [45] S. Javaid, M. J. Akhtar, Chem. Phys. Lett. 2016, 649, 73-77.
- [46] K. Tanikawa, K. Ohno, Y. Noda, S. Ono, R. Kuwahara, A. Takashima, M. Nakaya, J. Onoe, Chem. Phys. Lett. 2017, 686, 68-73.
- [47] E. J. G. Santos, W. L. Wang, Nanoscale 2016, 8, 1590215910.
- [48] M. A. L. Marques, E. K. U. Gross, Annu. Rev. Phys. Chem. 2004, 55, 427-455.
- [49] M. A. L. Marques, C. A. Ullrich, F. Nogueira, A. Rubio, K. Burke, E. K. U. Gross, *Time-dependent Density Functional Theory*, Springer, Berlin, 2006.
- [50] S. H. Vosko, L. Wilk, M. Nusair, Can. J. Phys. 1980, 58, 1200-1211.
- [51] A. D. Becke, *Phys. Rev. A* **1988**, *38*, 3098-3100.
- [52] C. Lee, W. T. Yang, R. G. Parr, *Phys. Rev. B* **1988**, 37, 785-789.
- [53] S. Grimme, J. Antony, S. Ehrlich, H. Krieg, J. Chem. Phys. 2010, 132, 154104.
- [54] P. J. Hay, W. R. Wadt, J. Chem. Phys. 1985, 82, 299-310.
- [55] T. H. Dunning Jr, J. Chem. Phys. 1989, 90, 1007-1023.
- [56] T. Yanai, D. P. Tew, N. C. Handy, *Chem. Phys. Lett.* **2004**, 393, 51-57.
- [57] T. Ziegler, A. Rauk, Theoret. Chim. Acta. 1977, 46, 1-10.
- [58] M. Mitoraj, A. Michalak, J. Mol. Model. 2007, 13, 347-355.
- [59] E. van Lenthe, E. J. Baerends, J. Comput. Chem. 2003, 24, 1142-1156.
- [60] I. G. Ryabinkin, J. Nagesh, A. F. Izmaylov, J. Phys. Chem. Lett. 2015, 6, 4200-4203.
- [61] X.-Y. Liu, X.-Y. Xie, W.-H. Fang, G. L. Cui, Mol. Phys. 2018, 116, 869-884.
- [62] G. Granucci, M. Persico, A. Zoccante, J. Chem. Phys. 2010, 133, 134111.
- [63] A. V. Akimov, A. J. Neukirch, O. V. Prezhdo, Chem. Rev. 2013, 113, 4496-4565.
- [64] X.-Y. Liu, Z.-W. Li, W.-H. Fang, G. L. Cui, J.Chem. Phys. 2018, 149, 044301.
- [65] X.-Y. Liu, Y.-H. Zhang, W.-H. Fang, G. L. Cui, J. Chem. Phys. A 2018, 122, 5518-5532.
- [66] S. Nosé, J. Chem. Phys. 1984, 81, 511-519.
- [67] W. G. Hoover, Phys. Rev. A 1985, 31, 1695-1697.
- [68] A. V. Akimov, O. V. Prezhdo, J. Am. Chem. Soc. **2014**, 136, 1599-1608.
- [69] A. V. Akimov, O. V. Prezhdo, J. Chem. Theory Comput. 2013, 9, 4959-4972.
- [70] Y.-G. Fang, L.-Y. Peng, X.-Y. Liu, W.-H. Fang, G. L. Cui, Comput. Theor. Chem. 2019, 1155, 90-100.

- [71] M. J. Frisch, G. W. Trucks, H. B. Schlegel, G. E. Scuseria, M. A. Robb, J. R. Cheesem, G. Scalmani, V. Barone, B. Mennucci, G. A. Petersson, H. Nakatsuji, M. Caricato, X. Li, H. P. Hratchian, A. F. Izmaylov, J. Bloino, G. Zheng, J. L. Sonnenberg, M. Hada, M. Ehara, K. Toyota, R. Fukuda, J. Hasegawa, M. Ishida, T. Nakajima, Y. Honda, O. Kitao, H. Nakai, T. Vreven, J. A. M. Jr., J. E. Peralta, F. Ogliaro, M. Bearpark, J. J. Heyd, E. Brothers, K. N. Kudin, V. N. Staroverov, R. Kobayashi, J. Normand, K. Raghavachari, A. Rendell, J. C. Burant, S. S. Iyengar, J. Tomasi, M. Cossi, N. Rega, J. M. Millam, M. Klene, J. E. Knox, J. B. Cross, V. Bakken, C. Adamo, J. Jaramillo, R. Gomperts, R. E. Stratmann, O. Yazyev, A. J. Austin, R. Cammi, C. Pomelli, J. W. Ochterski, R. L. Martin, K. Morokuma, V. G. Zakrzewski, G. A. Voth, P. Salvador, J. J. Dannenberg, S. Dapprich, A. D. Daniels, O. Farkas, J. B. Foresman, J. V. Ortiz, J. Cioslowski, D. J. Fox, Gaussian 09, Revision A.02. Gaussian, Inc., Wallingford CT, 2009.
- [72] G. te Velde, F. M. Bickelhaupt, E. J. Baerends, C. Fonseca Guerra, S. J. A. van Gisbergen, J. G. Snijders, T. Ziegler, J. Comput. Chem. 2001, 22, 931-967.
- [73] E. J. Baerends, T. Ziegler, A. J. Atkins, J. Autschbach, D. Bashford, A. Bérces, F. M. Bickelhaupt, C. Bo, P. M. Boerritger, L. Cavallo, D. P. Chong, D. V. Chulhai, L. Deng, R. M. Dickson, J. M. Dieterich, D. E. Ellis, M. van Faassen, L. Fan, T. H. Fischer, C. Fonseca Guerra, M. Franchini, A. Ghysels, A. Giammona, S. J. A. van Gisbergen, A. W. Götz, J. A. Groeneveld, O. V. Gritsenko, M. Grüning, S. Gusarov, F. E. Harris, P. van den Hoek, C. R. Jacob, H. Jacobsen, L. Jensen, J. W. Kaminski, G. van Kessel, F. Kootstra, A. Kovalenko, M. V. Krykunov, E. van Lenthe. D. A. McCormack, A. Michalak, M. Mitoraj, S. M. Morton, J. Neugebauer, V. P. Nicu, L. Noodleman, V. P. Osinga, S. Patchkovskii, M. Pavanello, C. A. Peeples, P. H. T. Philipsen, D. Post, C. C. Pye, W. Ravenek, J. I. Rodríguez, P. Ros, R. Rüger, P. R. T. Schipper, H. van Schoot, G. Schreckenbach, J. S. Seldenthuis, M. Seth, J. G. Snijders, M. Solá, M. Swart, D. Swerhone, G. te Velde, P. Vernooijs, L. Versluis, L. Visscher, O. Visser, F. Wang, T. A. Wesolowski, E. M. van Wezenbeek, G. Wiesenekker, S. K. Wolff, T. K. Woo, A. L. Yakovlev, ADF2016, SCM, Theoretical Chemistry, Vrije Universiteit, Amsterdam, The Netherlands, https://www.scm.com.
- [74] J. P. Perdew, K. Burke, M. Ernzerhof, Phys. Rev. Lett. 1996, 77, 3865-3868.
- [75] S. Goedecker, M. Teter, J. Hutter, *Phys. Rev. B* **1996**, *54*, 1703-1710.
- [76] C. Hartwigsen, S. Goedecker, J. Hutter, Phys. Rev. B 1998, 58, 3641-3662.
- [77] M. Krack, *Theor. Chem. Acc.* **2005**, *114*, 145-152.
- [78] J. VandeVondele, J. Hutter, J. Chem. Phys. 2007, 127, 114105.
- [79] J. VandeVondele, M. Krack, F. Mohamed, M. Parrinello, T. Chassaing, J. Hutter, Comput. Phys. Commun. 2005, 167, 103-128.
- [80] J. Hutter, M. lannuzzi, F. Schiffmann, J. VandeVondele, WIREs Comput. Mol. Sci. 2014, 4, 15-25.
- [81] G. L. Cui, W. Thiel, J. Chem. Phys. 2014, 141, 124101.
- [82] T. Lu, F. Chen, J. Comput. Chem. 2012, 33, 580-592.
- [83] A. Dreuw, M. Head-Gordon, J. Am. Chem. Soc. 2004, 126, 4007-4016.
- [84] J. C. Tully, R. K. Preston, J. Chem. Phys. 1971, 55, 562-572.
- [85] S. Hammes-Schiffer, J. C. Tully, J. Chem. Phys. 1994, 101, 4657-4667.
- [86] M.-E. Casida, J. Mol. Struct.: THEOCHEM 2009, 914, 3-18.
- [87] X. X. Chen, Z. J. Zhang, Z. C. Ding, J. Liu, L. X. Wang, Angew. Chem. Int. Ed. 2016, 128, 10532-10536.
- [88] J. H. Hou, Y. N. Wu, C. B. An, L. L. Shi, Z. H. Wang, Angew. Chem. Int. Ed. 2018, 57, 12911-12915.
- [89] R. Wang, C. F. Zhang, Q. Li, Z. G. Zhang, M. Xiao, J. Am. Chem. Soc. 2020, 142, 12751-12759.
- [90] C. Zhang, K. Nakano, M. Nakamura, F. Araoka, K. Tajima, D. Miyajima, J. Am. Chem. Soc. 2020, 142, 3326-3330.
- [91] H. F. Yao, L. Ye, H. Zhang, S. S. Li, S. Q. Zhang, J. H. Hou Chem. Rev. 2016, 116, 7397-7457.



